Published in final edited form as:
Cancer Res. 2011 March 15; 71(6): 2230–2239. doi:10.1158/0008-5472.CAN-10-1139.

Targeted signal amplifying enzymes enhance magnetic resonance imaging of EGFR expression in an orthotopic model of human glioma

Mohammed S. Shazeeb[1,3], **Christopher H. Sotak**[1,2,3], **Michael DeLeo III**[3], and **Alexei Bogdanov Jr**[3,4,#]

[1] Department of Biomedical Engineering, Worcester Polytechnic Institute Worcester, MA 01609

[2] Department of Chemistry & Biochemistry, Worcester Polytechnic Institute Worcester, MA 01609

[3] Department of Radiology, University of Massachusetts Medical School, 55 Lake Ave North, Worcester MA 01655

[4] Department of Cell Biology, University of Massachusetts Medical School, 55 Lake Ave North, Worcester MA 01655

Abstract

EGF receptor imaging in brain tumors is essential to visualize overexpression of EGFRvIII variants as a signature of highly aggressive gliomas and to identify patients that would benefit from anti-EGFR therapy. Seeking imaging improvements we tested a novel pretargeting approach that relies on initial administration of an enzyme-linked anti-EGFR mAb (EMD72000) followed by administration of a low-molecular weight paramagnetic molecule (diTyr-GdDTPA) retained at the site of EGFR mAb accumulation. We hypothesized that diTyr-GdDTPA would become enzyme-activated and retained on cells due to binding to tissue proteins. In support of this hypothesis, mAb-enzyme conjugates reacted with both membrane-isolated wild-type EGFR and EGFRvIII, but they bound primarily to EGFRvIII-expressing cells and not to EGFRwt-expressing cells. In vivo analysis of magnetic resonance (MR) tumor signal revealed differences in MR signal decay following diTyr-GdDTPA-substrate administration. These differences were significant in that they suggested differences in substrate elimination from the tissue which relied on the specificity of the initial mAb binding: a biexponential signal decay was observed in tumors only upon preinjection with EGFR-targeted conjugates. Endpoint MR imaging in this setting revealed detailed images of tumors which correlated with immunohistochemical detection of EGFR expression Together, our findings suggest an improved method to identify EGFRvIII-expressing gliomas in vivo that are bested suited for treatment with therapeutic EGFR antibodies.

Keywords

MRI; Molecular imaging; EGFR; glioma; kinetics; contrast agent

Introduction

Epidermal growth factor receptor (EGFR) is a member of ErbB receptor kinase family, which is overexpressed predominantly in non-small cell lung cancer, colorectal and

[#]Corresponding author: Dr. Alexei Bogdanov Departments of Radiology and Cell Biology, University of Massachusetts Medical School 55 Lake Ave North, Worcester MA 01655 Tel.508-856-5571 FAX 508-856-1860 Alexei.Bogdanov@umassmed.edu.

squamous carcinomas as well as in glioma cells (1–3). EGFR plays an important role in cancer pathogenesis by readily undergoing ligand-dependent dimerization followed by autophosphorylation of the EGFR dimer resulting in downstream proliferative and anti-apoptotic signaling in cancer cells (4). Wild-type EGFRwt overexpression closely correlates with receptor gene amplification and has been previously established as a significant and independent unfavorable predictor of overall survival of glioblastoma patients (5). The truncated EGFRvIII variant of the receptor is constitutively activated and is a hallmark of aggressive gliomas (6,7). Since EGFR level is low or even undetectable in normal brain cells, this receptor is an appealing molecular target not only for molecular therapies but also as a potential marker molecule for visualization and characterization of gliomas during their response to therapy. Several recombinant monoclonal antibodies (mAbs) have been developed during the past decade for achieving specific targeting of the N-terminal extracellular domain III of EGFR with the resultant inhibition of EGF binding and/or receptor dimerization (8–10). Anti-EGFR monoclonal antibodies (11,12) and EGF ligand (13,14) have recently been suggested as agents for targeted imaging of EGFR expression using near-infrared fluorescence. Unlike *in vivo* imaging of fluorescence, MRI does not suffer from the drawback of limited depth penetration and scattering of light. However, the sensitivity of MRI to the local molar concentration of contrast agent (CA) is orders of magnitude lower than fluorescence or radionuclide imaging, which limits applicability of MRI for receptor imaging (15–17). Proton MR receptor imaging relies on the ability of CAs associated with the receptor site to shorten relaxation times of nearby water molecules. The number of CA molecules, e.g. the number of chelated paramagnetic cations that can be used for direct labeling of mAbs while still maintaining the appropriate binding affinity of mAbs to the target site, is usually not sufficient for generating adequate MR contrast. Other studies circumvented the problem of insufficient sensitivity by coating iron oxides with mAbs (18–22), or by using gadolinium (Gd)-based targeted micelles (23) and dendrimers (24). MRI sensitivity is thus increased due to either clustering of many Gd cations or, alternatively, due to high superparamagnetism of iron oxide. However, linking of nano-sized CAs to antibodies can result in a decrease in tissue penetration after extravasation in tumors and in an increase of non-specific MR signal (25,26).

Several studies have looked into alternative uses of mAbs for imaging tumor-associated receptors using contrast-enhanced MRI (27–29). For example, a pre-targeting technique has been suggested for enhancing mammary adenocarcinomas by injecting Gd-labeled avidin (25) or dendrimers (29) as a way of achieving specific association with HER-2/*neu*-bound biotinylated mAb (trastuzumab) (28). We have previously developed a novel pre-targeting approach based on an enzyme-mediated amplification of MR signal as a result of accumulation of small molecular weight, Gd-labeled substrates at the target site (30). The advantage of this imaging strategy is that small CA molecules accumulate in brain tumors at a faster rate and with less heterogeneity than macromolecular agents (26). The resultant target-to-background contrast ratio can potentially be achieved earlier than in the case of nanoparticle or dendrimer pretargeting due to much faster elimination of the non-reacted CA substrate from the circulation as compared to non-bound Gd-labeled macromolecules or nanoparticles. The other potential advantage is in achieving higher MR signal due to the Gd relaxivity increase that results from the enzyme-activated substrate binding to proteins (31,32). The increase in relaxivity depends on magnetic field strength and strongly contributes to the MR signal increase at 1.0–2.0 Tesla.

The main goals of the current work were to: 1) test *in vitro* the tumor-pretargeted enzyme-mediated amplification system using cells expressing either EGFRwt, or both EGFRwt and EGFRvIII; 2) to compare *in vivo* kinetics of MR signal decay after the administration of Gd-labeled peroxidase substrate (diTyr-GdDTPA) with or without pre-targeting of the EGF receptor with mAb conjugated to a signal-amplification pair of enzymes.

Materials and Methods

Substrate synthesis and bioconjugation

Syntheses of HRP-reducing substrate di(tyramido)-DTPA(Gd) and conjugates (Fig. 1) was synthesized as described in (32); mAb conjugates were synthesized using bisaromatic hydrazone method, purified on Superdex200 HPLC columns (GE Life Sciences) and analyzed as described in (30).

Testing of conjugates in cell culture

Gli36ΔEGFR (33) and wild-type Gli36wt cells (34) were propagated on 10%FCS 90% RPMI1640 in the presence of penicillin/streptomycin and 0.5 μg/ml puromycin (Gli36ΔEGFR). mAb conjugates were cross-tittered on 96-well plated live cells using sequential dilutions in the range of 1000 – 7.5 ng total conjugate (i.e., a mixture of mAb-HRP and mAb-GOX) per well and peroxidase activity associated with the cells was determined as in (30).

Flow cytometry of Gli36ΔEGFR and Gli36wt cells was performed by using 1 μg/ml AlexaFluor488-labeled EMD72000 or cetuximab (humanized mAb C225 (35).

Internalization experiments

Cell Internalization was studied by using mAb-HRP/mAb-GOX conjugate mixture at 1:2 (w/w ratio). Adherent cells in 6-well plates (4 million cells/well) were incubated with conjugate mixtures either at 4°C or at 37°C. The surface bound conjugates were eluted with 0.5 ml cold 0.2M glycine, pH 2.5 for 15 min. The eluate was immediately neutralized with 1M Tris pH 8.0. To extract internalized conjugates 0.5 ml of 1.0% Igepal CA-630 in the presence of protease inhibitors was added to each well and plates incubated for 15 min. The amount of bound and internalized conjugates was determined by measuring the initial rates of HRP/GOX-coupled ABTS oxidation by adding of 5 mM ABTS, 5mM glucose (final concentrations) in sodium citrate, pH 5.5 to the sample aliquots and measuring absorbance at 405 nm over time. The serially diluted conjugate mixture at a constant mAb-HRP:mAb-GOX ratio and known concentrations was used for calibration.

Immunoblotting

Membrane proteins were extracted using CNM compartmental protein extraction procedure (BioChain Institute Inc., Hayward, CA) following manufacturer's recommendations with subsequent immunoblotting of protein-normalized lysates on PVDF membranes using either anti-EGFR mAb (ab3103, AbCam, Cambridge MA) as primary antibody or EMD72000-HRP conjugates with subsequent digital imaging.

Animal model

All procedures were performed as approved by the UMMS Institute Animal Care and Use Committee. An orthotopic human glioma xenograft model was obtained by stereotaxically implanting $1^{\cdot}10^{5}$ Gli36ΔEGFR or Gli36wt cells in 3 μl of 10% Matrigel™ in serum-free RPMI under aseptic conditions at 37°C (2.5 mm posterior to bregma, 2 mm lateral to midline, and depth of 3.5 mm) in the brain of athymic rats (Harlan, 150–180g, n=16) 14 d prior to the first imaging session. Throughout the imaging procedure the animals were maintained at 37°C and anesthetized using 1.5% isoflurane in a 30% oxygen/70% nitrogen mixture. A 45-mm-diameter, 30-mm-long birdcage RF coil was used. A 26-gauge catheter capped with a needle port was placed in the tail vein for CA administration.

MRI protocol, pulse sequences, and measurements

MRI measurements were performed using a Philips Achieva 3.0T/60 cm bore MRI scanner equipped with 80mT/m actively shielded gradients. To monitor temporal evolution of signal enhancement following CA delivery, multi-slice, T_1-WT MR images (TR/TE=700/8.2 ms) were acquired at various time-points following CA infusion. Other imaging parameters were: slice thickness = 1.5 mm; slice separation = 0.15 mm; field-of-view = 25.6 mm × 25.6 mm; data acquisition matrix = 256×128, 4 NEX. Two weeks after tumor cell implantation, each animal was imaged on two occasions: on Day 1 (two weeks after tumor cell implantation), a pre-contrast image was acquired followed by IV injection of 0.1 mmol/kg diTyr-GdDTPA. Twenty T_1-WT images were then acquired continuously over a 2-h period. On Day 2 (the day after Day 1), the animals were first pre-injected with 150 μg of mAb-HRP/mAb-GOX mixture at 2:1 (w/w ratio, 0.3 ml) in the tail vein. A separate group of Gli36ΔEGFR tumor animals were preinjected with non-specific antibody conjugates. Five hours later, a pre-contrast image was acquired followed by IV injection of 0.1 mmol/kg diTyr-GdDTPA. Thirty T_1-WT images were then acquired continuously over a 3-h period. Pre-contrast T_2-WT images were acquired on both Day 1 and Day 2 to corroborate the presence of tumor observed in the T_1-WT slices. The temporal evolution of the signal decay in the tumor following infusion of diTyr-GdDTPA was evaluated separately for each of the animal groups. Depending on the size of the tumor, one to four slices were selected. Image analysis was performed using ROIs for tumor interface and core regions with an aid of ImageJ software (36).

Histology

Following the MRI studies, animals were euthanized and their brains were removed. Under a dissecting microscope, histological slices were obtained ±2 mm anterior/posterior of the needle track and then embedded in O.C.T. medium. Frozen sections (6 μm) were fixed in acetone, treated by TBS/EDTA, pH 8 at 65°C for inhibiting endogenous phosphatase activity and blocked using 2% serum/TBS. The sections were incubated with anti-EGFR mouse mAb (Abcam), or anti-HRP mAb (Abcam) followed by anti-mouse alkaline-phosphatase linked antibodies and BCIP/NBT (Roche). Staining for residual peroxidase activity was achieved by using a DAB kit (Vector Labs). Immunofluorescent staining was performed on frozen sections blocked with 2% serum, 0.05% Tween-20, PBS, pH 7.4. AlexaFluor488-labeled EMD72000, Cy3-labeled mouse anti-rat CD31 mAb (clone TLD-3A12, Abcam, Cambridge MA) were used for visualizing EGFR and endothelial CD31 expression, respectively. For detecting HRP in the tissue sections, digoxigenin-labeled mouse anti-HRP mAb (clone 2H11, Abcam, Cambridge MA) was used. Digoxigenin-labeled antibody binding was visualized using custom Cy5.5-labeled anti-digoxigenin F(ab′)$_2$ (Roche, Indianapolis IN) (37).

Detailed methods are included in Supplemental Materials.

Results

Synthesis and testing of targeted MR signal amplification system in vitro

The synthesis of peroxidase (HRP) and glucose oxidase (GOX) conjugates of humanized chimeric antibody (EMD72000, Merck) that catalyze oligomerization of substrate di(tyramido)-DTPA(Gd) (Fig. 1) was performed using conditions optimized to facilitate enzyme conjugation with minimal antibody binding affinity loss (30). Gel electrophoresis of purified conjugates showed the formation of mAb-GOX (290 and 460 kD bands) and mAb-HRP (220 and 400 kD bands) (Fig. 2A). Since GOX is a two-subunit enzyme, the band corresponding to the 69 kD deglycosylated GOX subunit was present in the SDS-treated mAb-GOX conjugates (Fig. 2A, lane 4). The conjugation reaction conditions prevented the

formation of cross-linked products as evidenced by the lack of binding specificity to EGFR-positive cells. Immunoblotting experiments showed that optimized conjugates reacted with the same set of receptor variants (i.e. EGFRwt in Gli36wt and EGFRwt/EGFRvIII in Gli36ΔEGFR cell lysates) as did the control anti-EGFR antibody (Fig. 2Aa2). Overall, Gli36ΔEGFR cells contained 2.8-times more mAb-reactive EGF receptors than Gl36wt cells and this result correlated with the results of flow cytometry performed using fluorescent-labeled cetuximab (see Supplementary Fig. 1S, A). However, EMD72000 showed stronger preference for Gli36ΔEGFR cells, i.e., 7.2-times higher binding levels than Gli36wt cells (Supplementary Fig. 1S, B). Using ^{111}InDTPA-labeled EMD72000 mAb, we determined that Gli36ΔEGFR had $4.6\pm0.3\cdot10^5$ binding sites/cell as opposed to a control non-binding anti-EpCAM antibody, which showed no detectable binding to the surface of Gli36ΔEGFR cells. Optimization of the mAb-HRP:mAb-GOX conjugate ratios was performed to determine the conditions that provide sustainable release of hydrogen peroxide as a result of D-glucose oxidation, without inhibiting the binding of mAb-HRP to cells (see Supplementary Fig. 1S, B,C). These experiments showed no detectable loss of cell viability observed below 0.25 μg mAb-GOX/well. Cross-titration demonstrated that the highest HRP activity was detectable at the weight ratios of mAb-HRP:mAb-GOX of 1:2 in the range of 0.03(0.06) μg – 0.25(0.5) μg of mAb-GOX (mAb-HRP) conjugate/well. In contrast to Gli36ΔEGFR, the same dilutions of conjugates added to Gli36wt cells resulted in lower levels of cell-associated enzymatic activity. The titration of mAb-HRP:mAb-GOX conjugate mixture (1:2 w/w) allowed determination of the effective EC_{50} equal to 0.21 μg (Fig. 2C). Finally, we studied binding and internalization of optimized conjugate mixtures (Fig, 2D) in both cell lines by measuring the complementing enzymatic activities, which are essential for MR signal amplification. The differences observed during flow cytometry were further confirmed in these experiments showing that Gli36ΔEGFR cells were binding 10-times more of mAb conjugate-mediated enzymatic activity than Gli36wt, of which about 25% remained externalized on the surface of the cells.

The HRP/GOX mediated increase of relaxivity (i.e strength of MR CA) in the reaction mixture containing the paramagnetic substrate diTyr-GdDTPA was compared between low external magnetic field and the field of the MR imaging unit that was used for animal experiments. Mixtures of conjugates and paramagnetic substrate diTyr-GdDTPA in the presence of D-glucose always resulted in shorter T_1 relaxation times (i.e. higher average longitudinal relaxivity r1, see Supplementary Table S1). The measured difference in molar relaxivity between the substrate alone and reaction mixtures containing HRP and GOX conjugates was clearly greater at lower magnetic field (0.47T vs. 3T). The reaction resulted in 2.7 times higher r1 if measured at 0.47T as opposed to 5% increase of r1 at 3T. The simple addition of proteins in the solution did not result in large relaxivity gains. However, in the presence of both plasma proteins and mAb conjugates, the relaxivity increase was measurable and higher at 3T and showed a 20% r1 increase.

In vivo imaging experiments and corroboration

The paramagnetic-substrate-mediated enhancement of human glioma xenografts (Gli36ΔEGFR and Gli36wt) was studied using MRI *in vivo*. To account for tumor heterogeneity, the experiments were performed on consecutive days in each animal. On the first day, only the CA substrate was administered (Day 1). On the next day – after CA had been completely eliminated a–second experiment was conducted with pre-injection of mAb conjugates 5 h before injecting the CA (Day 2). Fig. 3A shows sequential T_1-WT rat brain MR images depicting Gli36ΔEGFR xenograft enhancement as a function of time post-IV injection of diTyr-GdDTPA. The top row of images shows the temporal washout of diTyr-GdDTPA with no anti-EGFR mAb conjugate pre-treatment (Day 1). The bottom row of images shows the temporal washout of diTyr-GdDTPA at 5 h following pre-treatment with

anti-EGFR mAb conjugates (Day 2) in the same slice for the same animal. For both days, the T_1-WT images showed strong initial enhancement of the tumor within minutes after IV diTyr-GdDTPA injection. However, following IV injection of diTyr-GdDTPA with EGFR-targeted conjugate pre-treatment (Fig. 3A: Day 2 – 8 min), the initial enhancement was significantly higher than without EGFR-targeted conjugate pre-treatment (Fig. 3A: Day 1 – 9 min), especially in the tumor interface region. Moreover, images obtained after the EGFR-targeted conjugate pre-injection (Fig. 3A: bottom row) showed more detailed tumor structure with areas of focal enhancement in both the tumor/normal brain interface and core at all time-points post-injection of the paramagnetic MR CA. With or without conjugate pre-treatment, the tumor interface consistently showed higher T_1-WT signal enhancement compared to the core.

Animals pre-injected with anti-EGFR mAb conjugates displayed a delayed retention of MR CA compared to animals not receiving EGFR-targeted conjugate pre-treatment. Without a pre-injection of anti-EGFR conjugates (Day 1), most of the diTyr-GdDTPA had washed out of both the tumor/normal brain interface and core regions by 117 minutes after IV injection (Fig. 3A: top row). However, after allowing the EGFR-targeted conjugates to accumulate in the tumors (Day 2), significant T_1-WT hyperintensity persisted in the tumor interface at approximately the same time point (Fig. 3A: Day 2 – 116 min) post-diTyr-GdDTPA-injection. Furthermore, T_1-WT enhancement in the tumor interface remained visible for 170 min after CA administration (Fig. 3A: Day 2 – 170 min). In contrast to EGFR-targeted conjugates pre-injection, no retention of MR signal was observed when Gli36ΔEGFR-bearing animals were pre-injected with anti-EpCAM targeted conjugates which do not bind to Gli36ΔEGFR cells (Fig. 3B: compare top and bottom rows).

The corroborative histology performed after the final MRI session showed areas of EGFR-positive staining and revealed two tumor masses (2.7–3 mm in diameter) with multiple microdeposits around the tumor/normal brain interface (arrows, Fig. 3D). These same features were also easily identifiable on MR images after the injection of anti-EGFR conjugate followed by the CA (Fig. 3C). These areas of tumor/brain were also positively stained for HRP activity using diaminobenzidine (Fig. 3D). By performing immunofluorescent visualization of EGFR and CD31 expression, we observed the presence of multiple blood vessels feeding the expanding tumor (Fig. 4A). Visualization of HRP accumulation by using anti-HRP antibodies (Fig. 4B) verified the results obtained using peroxidase enzymatic activity detection in brain sections (Fig. 3D).

Detailed kinetic analysis of *in vivo* MR signal enhancement as a function of time was performed to assess the efficacy of EGFR targeted imaging. Fig. 5 shows the normalized T_1-WT signal intensities in the Gli36ΔEGFR tumor interface and core regions as a function of time post-CA injection. These plots were derived from the tumor images of the same representative animals shown in Figs. 3A and 3B. The relative percent change in T_1-WT signal intensity of the interface and core regions was significantly higher with EGFR-targeted conjugate administration (Day 2, Fig. 5B) – as compared to without pre-treatment (Day 1, Fig. 5A) – at the initial time-points. With EpCAM-targeted conjugate administration (Day 2), there was no significant change in initial T_1-WT signal intensities of the interface and core regions between Day 1 and Day 2; both days showed similar washout behavior of the interface and core signal-intensity-decay curves (Fig. 5).

Interestingly, the signal-intensity-decay curves for tumor interface and core regions in animals pre-treated with EGFR-targeted conjugates (Day 2; Fig. 5B) depict two separate decay components (long τ_1 and shortτ_2) whereas the washout curves for the corresponding regions without EGFR-targeted conjugate injection (Day 1; Fig. 5A) show only a single decay component (τ_0). Based on the χ^2 analysis using an *F* test (Supplemental material), a

biexponential function was found to best model the signal-intensity-decay curves for the tumor interface and core regions after injection of EGFR-targeted conjugates (Day 2). Without EGFR-targeted conjugate preinjection (Day 1), a monoexponential function was found to best model both the regions. For treatment with and without EpCAM-targeted conjugates, and Gli36wt tumors (treated with and without EGFR-targeted conjugates), a monoexponential elimination function was the best model for all signal-intensity-decay curves (see Table 1 for all decay time constant (DTC) values).

Discussion

Imaging of receptor expression in cancer with high spatial resolution usually requires MR imaging assisted with imaging probes (38,39). Due to the inherent non-specific uptake of nano-sized probes in non-target cells and slow elimination of non-bound CA from blood, the specific imaging signal is frequently obscured. With a goal of imaging EGF receptor expression in gliomas, we investigated a novel strategy based on specific local retention of paramagnetic products of di(tyramido)-DTPA(Gd) (diTyr-GdDTPA, Fig. 1), i.e. a substrate of peroxidase (30,40). We applied the strategy in models of orthotopic human gliomas that either expressed the wild-type EGFR or both the wild type receptor and EGFRvIII (33). The anti-EGFR mAb (EMD72000) was covalently linked with HRP and GOX, i.e. to the enzymes that function as a self-complementing enzymatic signal amplification system (30). In cell culture experiments, these conjugates showed a remarkable preference for truncated EGFRvIII mutant form expressed in Gli36ΔEGFR cells but not in Gli36wt counterpart. This effect can be explained by the steric constraints in accessibility of epitope (Ser460-Gly461) on EGFR domain III recognized by EMD72000 antibody (41). Since even after prolonged incubation in cell culture 25% of mAb conjugates were resistant to internalization, we anticipated that our strategy enables reliable MR imaging of EGFRvIII with high specificity due to the retention of CA at the sites of mAb conjugate co-localization.

To test this assumption, we designed experiments that directly compared *in vivo* elimination kinetics of diTyr-GdDTPA in the same tumor-bearing animals. These experiments were performed initially in the absence of mAb conjugates and then after the pre-injection of a mixture of conjugates at the optimized HRP:GOX ratio. As a result, we were able to compare kinetics of the measured MR signal decrease due to the washout of diTyr-GdDTPA and its reactive products from the total tumor volume, as well as from volumes corresponding to highly vascularized tumor “interface” (Fig. 4 and Supplementary Fig. 2S) and the remaining “core” volumes. From the quantitative kinetic analysis of the MR signal intensities, we concluded that the initial MR signal intensity enhancement for both interface and core regions was significantly higher for Gli36ΔEGFR tumors that were pre-treated with EGFR-targeted mAb conjugates (Day 2) as compared to the same tumors before the injection of conjugates (Day 1), or Gli36wt tumors. When non-targeted mAb conjugates (control) were preinjected into Gli36ΔEGFR tumors, no significant signal change was observed compared to Day 1. Binding of paramagnetic products of enzymatic reaction are more efficient contrast agents and their binding to the EGFRvIII-positive tumors resulted in a long-term retention/enhancement (Fig. 3A), while oligomerization or binding to proteins in the extracellular compartment resulted in a short-term tumor enhancement. The effects caused by paramagnetic products binding were previously observed and characterized in several similar enzyme-mediated reactions (32,42).

The retention of MR signal enhancement in tumors that were pre-treated with specific targeted conjugates relative to those that were not, resulted in a slower CA elimination consistent with the binding of the CA to the target cells in the presence of targeted enzyme amplification pair. As expected, signal enhancement of the tumor interface was initially higher than that of the rest of the tumor volume (“core”), independent of whether the

animals were preinjected with conjugates or not. This was caused by high vascular density of the tumor interface (Fig. 3), which corresponds to an area of enhanced transvascular permeability and higher functional blood volume (43). The higher local permeability translates into higher concentrations of targeted conjugates as well as the substrate compared to less vascularized core. The results of direct staining for HRP activity or detection of HRP in tumors by using immunofluorescence suggest this difference (Figs. 3 and 4).

The inevitable variations in tumor size and tumor heterogeneity dictated the need in a parameter that would allow comparing MR imaging results obtained in different animals and tumors. We determined that kinetic analysis of temporal decay of the normalized MR signal intensities can be used for this purpose (Table 1). The calculated DTC values can be correlated to tumor perfusion, vascular permeability, and the volume of the extravascular extracellular space (EES) (see Supplemental material).

By performing signal intensity decay analysis we found that in the absence of conjugate preinjection, the washout of diTyr-GdDTPA was monoexponential throughout the tumor volume generating a single DTC (τ_0) in both tumor models (Fig. 5A; Table 1). In each case τ_0 was attributed to the washout of the free CA since the substrate does not bind to plasma proteins. This assignment is justified because diTyr-GdDTPA is not expected to have any affinity for tumor cells in the absence of receptor-targeted conjugates. The control EpCAM-targeted conjugates in Gli36ΔEGFR tumors (Day 2) as well as EGFR-targeted conjugates in Gli36wt cells (Day 2) similarly showed monoexponential decay (Table 1) since control anti-EpCAM conjugates did not bind to glioma cells of our study and Gli36wt cells were binding very low amounts of EMD72000 conjugates.

Following the pre-injection of Gli36ΔEGFR-bearing animals with EGFR-targeted conjugates on Day 2, the diTyr-GdDTPA elimination changed from monoexponential to biexponential for both the tumor interface and core regions (Fig. 5; Table 1). The elimination of free (and/or oligomerized) substrate was responsible for short DTC (τ_2) while the long DTC (τ_1) component was attributed to paramagnetic reaction products retained by tumor cells. Importantly, the comparison of τ_1 and τ_2 DTC values suggest that in addition to dynamic acquisition delayed MR imaging can also be useful when imaging receptors: the retention of tumor bound paramagnetic product resulting from a specific enzymatic reaction can be detectable in the tumor interface for several hours post administration of the substrate while the free substrate is eliminated within an hour.

In conclusion, we performed quantitative analysis of MR dynamic signal enhancement in human glioma xenografted animals that were: 1) imaged first by using “non-specific” paramagnetic CA; 2) imaged with the same CA after preinjecting of anti-EGFR antibody conjugates. The enzyme linked to EGFR-targeted antibodies converted the CA into reactive products thereby profoundly changing the tissue elimination kinetics. Therefore, in addition to imaging of the MR signal enhancement associated with tumor tissues *in vivo* the amplification strategy results in a kinetic signature. The analysis of images acquired dynamically or by using end point imaging can establish the presence of cell surface marker and quickly delineate the areas where this marker molecule can be targeted for therapeutic purposes.

Supplementary Material

Refer to Web version on PubMed Central for supplementary material.

Acknowledgments

This work was supported by 5R01EB000858 grant to AB. We are grateful to Dr. Suresh Gupta, Jamie O'Callaghan and Dr. Hye-Won Kang for assistance with several aspects of this work, including cell culture experiments and animal surgery. We acknowledge Merck KGaA (Darmstadt, Germany) for providing EMD72000 antibody. We are grateful to Dr. Mary Mazzanti for editing the text.

References

1. Bigner SH, Humphrey PA, Wong AJ, et al. Characterization of the epidermal growth factor receptor in human glioma cell lines and xenografts. Cancer Res. 1990; 50:8017–22. [PubMed: 2253244]
2. Sauter G, Maeda T, Waldman FM, Davis RL, Feuerstein BG. Patterns of epidermal growth factor receptor amplification in malignant gliomas. Am J Pathol. 1996; 148:1047–53. [PubMed: 8644846]
3. Schwechheimer K, Huang S, Cavenee WK. EGFR gene amplification--rearrangement in human glioblastomas. Int J Cancer. 1995; 62:145–8. [PubMed: 7622287]
4. Schlessinger J. Ligand-induced, receptor-mediated dimerization and activation of EGF receptor. Cell. 2002; 110:669–72. [PubMed: 12297041]
5. Shinojima N, Tada K, Shiraishi S, et al. Prognostic value of epidermal growth factor receptor in patients with glioblastoma multiforme. Cancer Res. 2003; 63:6962–70. [PubMed: 14583498]
6. Ekstrand AJ, Longo N, Hamid ML, et al. Functional characterization of an EGF receptor with a truncated extracellular domain expressed in glioblastomas with EGFR gene amplification. Oncogene. 1994; 9:2313–20. [PubMed: 8036013]
7. Nishikawa R, Ji XD, Harmon RC, et al. A mutant epidermal growth factor receptor common in human glioma confers enhanced tumorigenicity. Proc Natl Acad Sci USA. 1994; 91:7727–31. [PubMed: 8052651]
8. Ciardiello F. Epidermal growth factor receptor inhibitors in cancer treatment. Future Oncol. 2005; 1:221–34. [PubMed: 16555994]
9. Wagner TD, Yang GY. Cetuximab: its use in combination with radiation therapy and chemotherapy in the multimodality treatment of head and neck cancer. Recent Pat Anticancer Drug Discov. 2008; 3:76–83. [PubMed: 18537749]
10. Weber J, McCormack PL. Panitumumab: in metastatic colorectal cancer with wild-type KRAS. BioDrugs. 2008; 22:403–11. [PubMed: 18998757]
11. Gleysteen JP, Newman JR, Chhieng D, Frost A, Zinn KR, Rosenthal EL. Fluorescent labeled anti-EGFR antibody for identification of regional and distant metastasis in a preclinical xenograft model. Head Neck. 2008; 30:782–9. [PubMed: 18228526]
12. Koyama Y, Barrett T, Hama Y, Ravizzini G, Choyke PL, Kobayashi H. In vivo molecular imaging to diagnose and subtype tumors through receptor-targeted optically labeled monoclonal antibodies. Neoplasia. 2007; 9:1021–9. [PubMed: 18084609]
13. Adams KE, Ke S, Kwon S, et al. Comparison of visible and near-infrared wavelength-excitable fluorescent dyes for molecular imaging of cancer. J Biomed Opt. 2007; 12:024017. [PubMed: 17477732]
14. Diagaradjane P, Orenstein-Cardona JM, Colon-Casasnovas NE, et al. Imaging epidermal growth factor receptor expression in vivo: pharmacokinetic and biodistribution characterization of a bioconjugated quantum dot nanoprobe. Clin Cancer Res. 2008; 14:731–41. [PubMed: 18245533]
15. Nunn AD, Linder KE, Tweedle MF. Can receptors be imaged with MRI agents? Q J Nucl Med. 1997; 41:155–62. [PubMed: 9203854]
16. Rudin M, Weissleder R. Molecular imaging in drug discovery and development. Nat Rev Drug Discov. 2003; 2:123–31. [PubMed: 12563303]
17. De Leon-Rodriguez LM, Lubag AJ, Malloy CR, Martinez GV, Gillies RJ, Sherry AD. Responsive MRI agents for sensing metabolism in vivo. Acc Chem Res. 2009; 42:948–57. [PubMed: 19265438]
18. Cerdan S, Lotscher HR, Kunnecke B, Seelig J. Monoclonal antibody-coated magnetite particles as contrast agents in magnetic resonance imaging of tumors. Magn Reson Med. 1989; 12:151–63. [PubMed: 2615625]

19. To SY, Castro DJ, Lufkin RB, Soudant J, Saxton RE. Monoclonal antibody-coated magnetite particles as contrast agents for MR imaging and laser therapy of human tumors. J Clin Laser Med Surg. 1992; 10:159–69. [PubMed: 10147859]
20. Remsen LG, McCormick CI, Roman-Goldstein S, et al. MR of carcinoma-specific monoclonal antibody conjugated to monocrystalline iron oxide nanoparticles: the potential for noninvasive diagnosis. AJNR Am J Neuroradiol. 1996; 17:411–8. [PubMed: 8881233]
21. Suwa T, Ozawa S, Ueda M, Ando N, Kitajima M. Magnetic resonance imaging of esophageal squamous cell carcinoma using magnetite particles coated with anti-epidermal growth factor receptor antibody. Int J Cancer. 1998; 75:626–34. [PubMed: 9466667]
22. Yang L, Mao H, Wang YA, et al. Single chain epidermal growth factor receptor antibody conjugated nanoparticles for in vivo tumor targeting and imaging. Small. 2009; 5:235–43. [PubMed: 19089838]
23. Nasongkla N, Bey E, Ren J, et al. Multifunctional polymeric micelles as cancer-targeted, MRI-ultrasensitive drug delivery systems. Nano Lett. 2006; 6:2427–30. [PubMed: 17090068]
24. Kobayashi H, Brechbiel MW. Nano-sized MRI contrast agents with dendrimer cores. Adv Drug Deliv Rev. 2005; 57:2271–86. [PubMed: 16290152]
25. Netti PA, Hamberg LM, Babich JW, et al. Enhancement of fluid filtration across tumor vessels: implication for delivery of macromolecules. Proc Natl Acad Sci USA. 1999; 96:3137–42. [PubMed: 10077650]
26. Neuwelt EA, Specht HD, Hill SA. Permeability of human brain tumor to 99mTc-gluco-heptonate and 99mTc-albumin. Implications for monoclonal antibody therapy. J Neurosurg. 1986; 65:194–8. [PubMed: 3723177]
27. Artemov D, Mori N, Okollie B, Bhujwalla ZM. MR molecular imaging of the Her-2/neu receptor in breast cancer cells using targeted iron oxide nanoparticles. Magn Reson Med. 2003; 49:403–8. [PubMed: 12594741]
28. Artemov D, Mori N, Ravi R, Bhujwalla ZM. Magnetic resonance molecular imaging of the HER-2/neu receptor. Cancer Res. 2003; 63:2723–7. [PubMed: 12782573]
29. Zhu W, Okollie B, Bhujwalla ZM, Artemov D. PAMAM dendrimer-based contrast agents for MR imaging of Her-2/neu receptors by a three-step pretargeting approach. Magn Reson Med. 2008; 59:679–85. [PubMed: 18302223]
30. Bogdanov A Jr, Kang HW, Querol M, Pretorius PH, Yudina A. Synthesis and testing of a binary catalytic system for imaging of signal amplification in vivo. Bioconjug Chem. 2007; 18:1123–30. [PubMed: 17508710]
31. Bogdanov A Jr, Matuszewski L, Bremer C, Petrovsky A, Weissleder R. Oligomerization of paramagnetic substrates result in signal amplification and can be used for MR imaging of molecular targets. Mol Imaging. 2002; 1:16–23. [PubMed: 12920857]
32. Querol M, Bennett DG, Sotak C, Kang HW, Bogdanov A Jr. A paramagnetic contrast agent for detecting tyrosinase activity. Chembiochem. 2007; 8:1637–41. [PubMed: 17694521]
33. Ichikawa T, Hogemann D, Saeki Y, et al. MRI of transgene expression: correlation to therapeutic gene expression. Neoplasia (New York). 2002; 4:523–30.
34. Sena-Esteves M, Saeki Y, Camp SM, Chiocca EA, Breakefield XO. Single-step conversion of cells to retrovirus vector producers with herpes simplex virus-Epstein-Barr virus hybrid amplicons. J Virol. 1999; 73:10426–39. [PubMed: 10559361]
35. Masui H, Kawamoto T, Sato JD, Wolf B, Sato G, Mendelsohn J. Growth inhibition of human tumor cells in athymic mice by anti-epidermal growth factor receptor monoclonal antibodies. Cancer Res. 1984; 44:1002–7. [PubMed: 6318979]
36. Rasband, W. Health USNIo. ImageJ. Bethesda, MD, USA: 1997–2010. http://rsb.info.nih.gov/ij/
37. Petrovsky A, Schellenberger E, Josephson L, Weissleder R, Bogdanov A Jr. Near-infrared fluorescent imaging of tumor apoptosis. Cancer Res. 2003; 63:1936–42. [PubMed: 12702586]
38. Reimer P, Weissleder R, Lee AS, Wittenberg J, Brady TJ. Receptor imaging: application to MR imaging of liver cancer. Radiology. 1990; 177:729–34. [PubMed: 2243978]
39. Weissleder R, Moore A, Mahmood U, et al. In vivo magnetic resonance imaging of transgene expression. Nat Med. 2000; 6:351–5. [PubMed: 10700241]

40. Querol M, Bogdanov A Jr. Amplification strategies in MR imaging: activation and accumulation of sensing contrast agents (SCAs). J Magn Reson Imaging. 2006; 24:971–82. [PubMed: 17024658]

41. Kamat V, Donaldson JM, Kari C, et al. Enhanced EGFR inhibition and distinct epitope recognition by EGFR antagonistic mAbs C225 and 425. Cancer Biol Ther. 2008; 7:726–33. [PubMed: 18424917]

42. Rodriguez E, Nilges M, Weissleder R, Chen JW. Activatable magnetic resonance imaging agents for myeloperoxidase sensing: mechanism of activation, stability, and toxicity. J Am Chem Soc. 2009; 132:168–77. [PubMed: 19968300]

43. JuanYin J, Tracy K, Zhang L, et al. Noninvasive imaging of the functional effects of anti-VEGF therapy on tumor cell extravasation and regional blood volume in an experimental brain metastasis model. Clin Exp Metastasis. 2009; 26:403–14. [PubMed: 19277878]

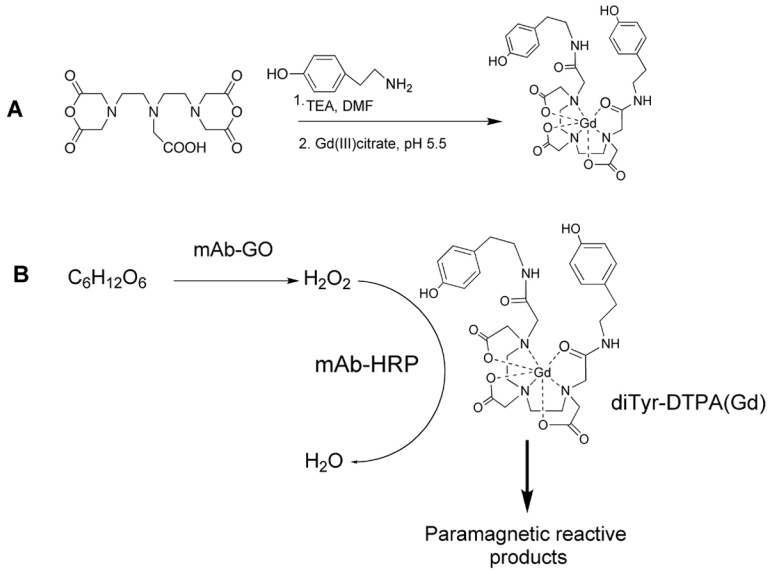

Figure 1.

A– Synthesis of peroxidase-reducing paramagnetic substrate di(tyramido)-DTPA(Gd); **B–** Reaction of diTyr-GdDTPA with the peroxidase/glucose oxidase enzyme pair conjugated to anti-EGFR mAb.

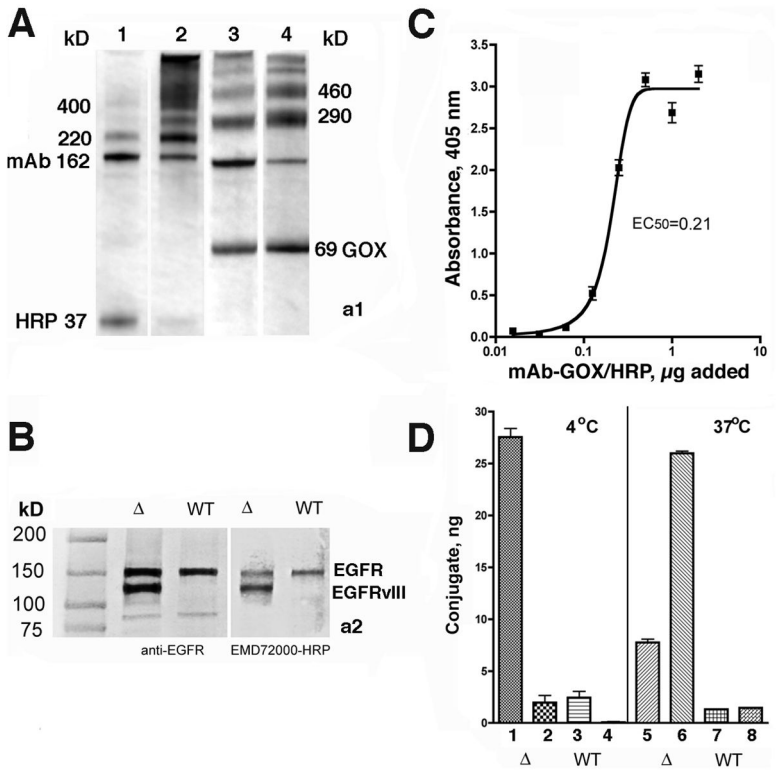

Figure 2.

A– SDS-PAGE (4–15% gradient) of anti-EGFR mAb (EMD72000) conjugation products or with deglycosylated enzymes: HRP (37 kD, lanes 1 and 2) and with GOX (69 kD subunit, lanes 3, 4) Lanes 1 and 3- before and 2,4- after the purification of conjugates; **B**– immunoblotting of membrane proteins isolated from Gli36ΔEGFR (Δ) and Gli36wt (WT) cells using mouse monoclonal anti-EGFR antibody C225 or by using HRP-EMD72000 conjugate. EGFR variants are identified on the right; **C –** titration of the mixture of anti-EGFR mAb-HRP and mAb-GOX on Gli36ΔEGFR cells at the optimized complementing ratio (1:2, w/w); **D –** binding and internalization of conjugate mixture at the optimized ratio (1:2, w/w) in Gli36ΔEGFR (Δ) and Gli36wt (WT) cells 1,3, 5,7 – cell-surface bound fraction of conjugates; 2,4,6,8 – internalized fraction of conjugates.

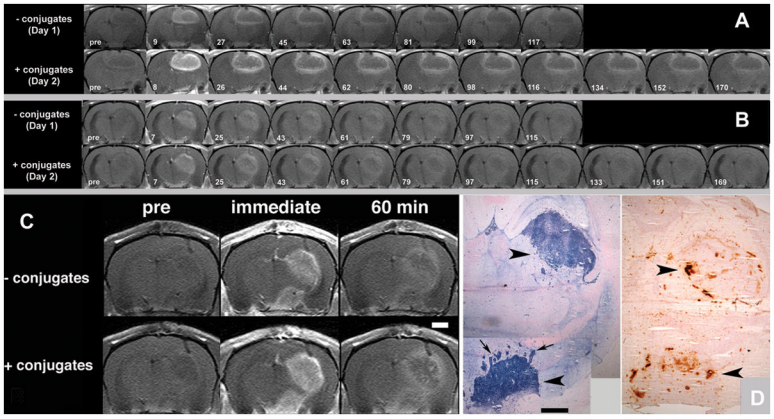

Figure 3.

A – 3T MR imaging of Gli36ΔEGFR human glioma xenografts without and with pre-injection of EGFR-targeted conjugates. T_1-WT sequential rat brain images depicting enhancement as a function of time post injection of diTyr-GdDTPA; Top row -temporal washout of diTyr-GdDTPA with no conjugate pre-injection (Day 1); Bottom row - washout of diTyr-GdDTPA following pre-treatment with anti-EGFR conjugates (Day 2) in the same slice for the same animal. Time intervals (in minutes) after the injection of diTyr-GdDTPA are shown below; **B** – Gli36ΔEGFR xenografts without and with pre-injection of EpCAM-targeted conjugates. The images correspond to the same pattern as shown in Panel A; **C** – MRI and comparative histology. The images were obtained pre-, immediately post- and 1 h post- diTyr-GdDTPA administration; **D** – Left: Detection of EGFR overexpression using anti-EGFR antibody-digoxigenin/anti-digoxigenin-AP system in the tumor shown in Fig. 3C; Right: Detection of HRP activity in the same tumor on the parallel section using diaminobenzidine staining. Arrowheads point to tumor location; arrows show presence of tumor expansion as microdeposits in normal brain tissue stained for EGFR expression. Bars in B, C = 1 mm.

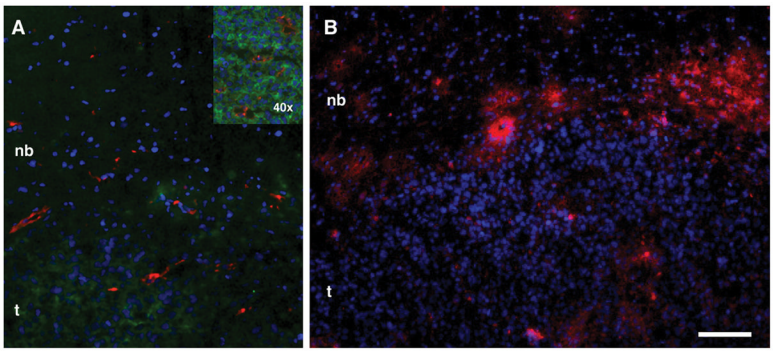

Figure 4.

Immunofluorescent detection of EGF receptor, endothelial cells and mAb conjugate delivery in Gli36ΔEGFR tumors. **A** – Detection of EGFR expression (green) and blood vessels (anti-CD31, red). The inset shows area of vascularized tumor/brain interface at higher magnification; **B** – Binding of anti-EGFR-HRP conjugate to cells in the tumor interface after injection. Binding of digoxigenin-labeled anti-HRP antibody (detected by using anti-digoxigenin $F(ab')_2$-Cy5.5 conjugate) is shown in red. Nuclei are stained with DAPI. Bar 50 μm. t- tumor, nb- normal brain.

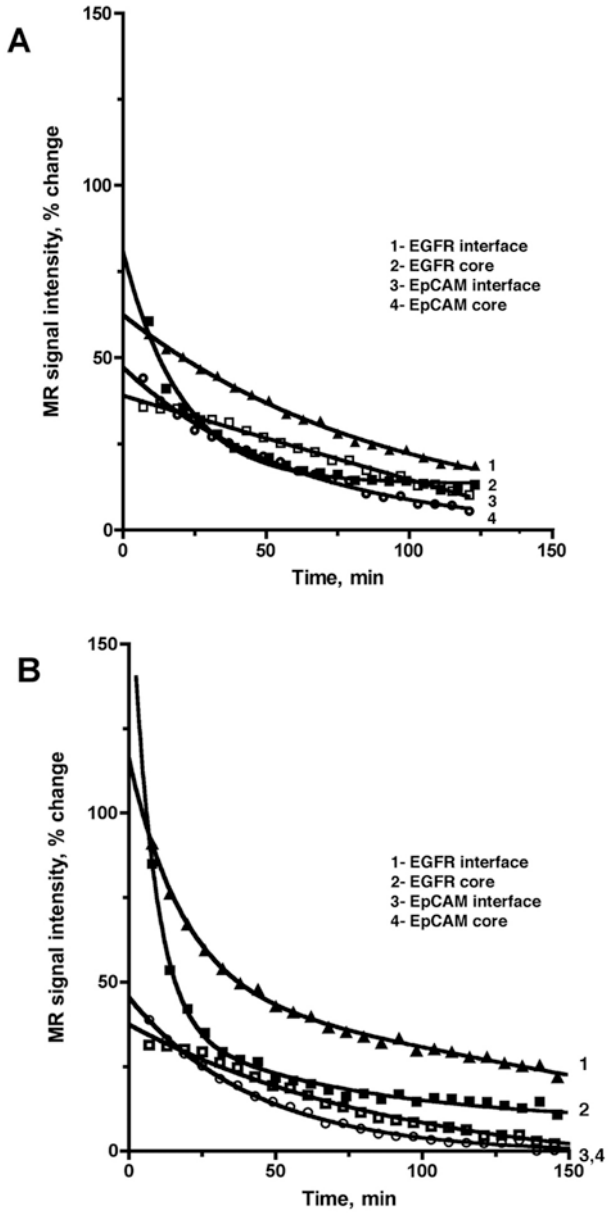

Figure 5.

Normalized T_1-WT signal intensities measured in the interface or core regions of the representative Gli36ΔEGFR tumors prior to injection of conjugates (**A**), or after the pre-injection of either specific anti-EGFR (“EGFR”) or non-specific EpCAM (“EpCAM”) conjugates (**B**) as a function of time post-diTyr-GdDTPA injection. The signal intensities are normalized as percent change relative to the pre-contrast image. MR signal showed biexponential decay in tumors of animals pre-injected with anti-EGFR conjugates (B, curves 1,2) whereas the MR signal decay curves with no conjugate pre-injection or after the pre-injection of non-specific conjugate (A, curves 1–4, B curves 3,4) showed a single (monoexponential) decay.

Table 1

Decay time constants (DTC) for diTyr-GdDTPA or its products in the tumor interface and core regions with (Day 2) or without conjugate pre-injection (Day 1).

	Gli36ΔEGFR tumors, EMD72000 (anti-EGFR) conjugates (experiment)				**Gli36ΔEGFR tumors, anti-EpCAM conjugates (control)**		**Gli36-WT tumors, EMD72000 conjugates (control)**
	Tumor core DTC (min) *a)*		**Tumor interface DTC (min)** *a)*		**Tumor core DTC (min)** *a)*	**Tumor interface DTC (min)** *a)*	**Tumor core DTC (min)** *a)*
No preinjection of conjugates (Day 1)		**τ_0 (min)** *b)*		**τ_0 (min)** *b)*	**τ_0 (min)** *b)*	**τ_0 (min)** *b)*	**τ_0 (min)** *b)*
		36 ± 10 *j)*		54 ± 20 *j)*	54 ± 28	92 ± 46	43 ± 4
With pre- injection of conjugates (Day 2)	**τ_1 (min)** *c)*	**τ_2 (min)** *c)*	**τ_1 (min)** *c)*	**τ_2 (min)** *c)*	**τ_0 (min)** *d)*	**τ_0 (min)** *d)*	**τ_0 (min)** *e)*
	102 ± 32	11 ± 7 *k)*	133 ± 47	25 ± 10 *k)*	36 ± 6	103 ± 49	55 ± 3
P values	P < 0.005 *f)*	P < 0.0002 *g)*	P < 0.009 *h)*	P < 0.004 *i)*	NS *m)*	NS *m)*	P < 0.05 *l)*

a) Region of interest placement is explained in Supplementary Fig. 2S;

b) monoexponential fitting model was used;

c) values in shaded area - biexponential fitting of signal-intensity-decay (SID) curves. A monoexponential function was used for the tumor regions in animals with:

d) Gli36ΔEGFR group pre-injected with EpCAM conjugates (Day 2);

e) Gli36-WT group pre-injected with anti-EGFR (EMD72000) conjugates (Day 2).

P values correspond to comparisons within Gli36ΔEGFR group (preinjected with EMD72000 conjugates) between:

f) τ_0 and τ_1 in the tumor core;

g) τ_0 and τ_2 in the tumor core;

h) τ_0 and τ_1 in the tumor interface;

i) τ_0 and τ_2 in the tumor interface;

j) P < 0.01 for τ_0 values in the tumor core and interface;

k) P < 0.03 for τ_2 values in the tumor core and interface;

l) P value corresponds to comparisons between τ_0 values in the tumor core region of animals with Gli36-WT tumors (preinjected with EMD72000 conjugates);

m) No significant differences in DTCs were observed in the tumor regions between Day 1 and Day 2 in animals with Gli36ΔEGFR group preinjected with EpCAM conjugates.